A Level Set Based Flamelet Model for the Prediction of Combustion in Spark Ignition Engines

Jens Ewald, Norbert Peters
Institut für Technische Mechanik, RWTH Aachen University
Templergraben 64, D–52056 Aachen, Germany
E-Mail: j.ewald@itm.rwth-aachen.de

Abstract

A Flamelet Model based on the Level Set approach for turbulent premixed combustion is presented. The original model [11, 12] is enhanced in order to consistently model the evolution of the premixed flame from laminar into a fully developed turbulent flame. This is accomplished by establishing a linear relationship between the thickness of the turbulent flame brush and the turbulent burning velocity. Starting from there a model for the initial flame propagation of a spherical spark kernel immediately after ignition and for the flame propagation in 3D space is derived. In contrast to other models, the same physical modeling assumptions are employed for the phase initially after spark ignition and for the later phases of flame propagation. The model is applied to a test case in an homogeneous charge Spark Ignition (SI) engine.

Introduction

With respect to laminar premixed flames, Williams [19] postulated a kinematic equation for the advection of the laminar flame based on the scalar G. The laminar approach then was subsequently extended by Peters [10] to turbulent premixed flames. Due to the kinematic Level Set approach employed, the turbulent burning velocity s_T is model input into the kinematic equation and not a reaction rate defined per unit volume. This approach therefore overcomes problems in case that the (laminar or turbulent) flame thickness becomes small in comparison to the numerical grid used in the problem simulation and in that limit, the reaction rate would become a delta peak, which is difficult to be integrated numerically. Furthermore the interaction of the different physical phenomena of diffusion and reaction that establish the structure of the premixed flame are physically correctly represented by employing the burning velocity which is an eigenvalue of the premixed problem posed [9].

The first turbulent combustion model was then refined [11] by sub-dividing the flamelet combustion regime into the corrugated flamelets regime, in which large scale turbulence is active and the thin reaction zones regime, in which small scale turbulence dominates. In the latter regime, the smallest turbulent scales act on the laminar flamelet. This is the cause of the so-called bending effect, by which a decrease of the turbulent burning velocity is predicted for smaller Damköhler numbers.

The turbulent G-Equation concept was already successfully used for Spark Ignition (SI) Engine applications, cf. Dekena *et al.* [5] or Tan *et al.* [16, 15]. In these works, two different models, one for spark ignition and the phase immediately thereafter, and the other for the propagation of the fully turbulent developed flame at later stages of the combustion process were used. The spark ignition models in both cases predict lower turbulent burning velocities for the developing turbulent flame kernel than the turbulent burning velocity expression in [11] which assumes a fully developed flame. After a user given time period, the models are switched to the latter model equation.

In this work, a unified approach for the flame propagation during the phase immediately after ignition and one the turbulent flame is developed is presented. The key idea is to consistently relate the thickness of the turbulent flame brush to the turbulent burning velocity. Immediately after ignition the thickness of the turbulent flame brush is zero – except for the laminar flame thickness – and laminar flame propagation is predicted.

The unified approach then is cast into two different numerical representations, one for the numerical integration in 3D space on the numerical grid of the problem. The other representation assumes the spark kernel to be spherical which allows for a grid-independent description of the developing spark, therefore overcoming to a certain extent the necessity to refine the computational grid at the position of ignition. Also, due to the geometry of the spark kernel assumed, effects of kernel curvature can easily be assessed.

Unsteady Premixed Combustion Model

The turbulent premixed combustion flamelet model by Peters [11, 12] is based on three quantities which are $\widetilde{G}$, the mean flame front position, the variance of the flame brush

$\widetilde{G''^2} = \ell_{f,t}^2$ which is related to the turbulent flame thickness $\ell_{f,t}$, and the turbulent flame surface area ratio $\widetilde{\sigma}_t$.

At the mean flame front position $\widetilde{G} = G_0$, the kinematic equation

$$\langle\rho\rangle \frac{\partial \widetilde{G}}{\partial t} + \langle\rho\rangle \nabla\widetilde{G}\cdot\widetilde{\vec{u}} = \langle\rho\rangle D'_t \widetilde{\kappa}|\nabla\widetilde{G}| + \widetilde{(\rho s_T)}|\nabla\widetilde{G}| \quad (1)$$

is applied while outside of this surface the distance constraint $|\nabla\widetilde{G}| = 1$ is imposed. Since eqn. (1) is pertinent to the class of Level Sets, appropriate numerical solving techniques need to be employed, cf. [2, 13, 8]. The two terms on the r.h.s. are due to the modeling of the turbulent flame propagation. The last term describes the averaged turbulent mass burning rate $\widetilde{(\rho s_T)}$ and the first influences due to curvature $\widetilde{\kappa} \equiv \nabla\cdot(\nabla\widetilde{G}/|\nabla\widetilde{G}|)$ of the mean front.

The equation for the variance is modeled in analogy to the variance equation for a passive scalar [12]

$$\begin{aligned}\langle\rho\rangle \frac{\partial \widetilde{G''^2}}{\partial t} + \langle\rho\rangle \nabla\widetilde{G''^2}\cdot\widetilde{\vec{u}} &= \nabla\cdot\left(\langle\rho\rangle D_t \nabla\widetilde{G''^2}\right) \\ &+2\langle\rho\rangle D_t(\nabla\widetilde{G})^2 - c_s\langle\rho\rangle \widetilde{G''^2}\frac{\varepsilon}{k}\end{aligned} \quad (2)$$

with the last two terms on the r.h.s. being the turbulent production and dissipation, respectively.

The relationship between the turbulent burning velocity s_T and the flame propagation of the laminar flamelet s_L is established by $\widetilde{\sigma}_t$ as:

$$s_T = (1+\widetilde{\sigma}_t)s_L\ . \quad (3)$$

Here, $\widetilde{\sigma}_t$ is determined by an algebraic equation to be

$$\begin{aligned}\widetilde{\sigma}_t = \frac{\ell_{f,t}}{\ell_f}\Bigg\{ &-\frac{b_3^2}{4b_1}\sqrt{\frac{3c_\mu c_s}{\mathrm{Sc}_t}} \\ &+\sqrt{\frac{b_3^4}{16b_1^2}\frac{3c_\mu c_s}{\mathrm{Sc}_t} + \frac{c_s b_3^2}{2}\frac{\ell_f}{s_L}\frac{\varepsilon}{k}}\Bigg\}\ ,\end{aligned} \quad (4)$$

which establishes a linear relationship between the ratio of the turbulent to laminar flame thickness $\ell_{f,t}/\ell_f$ and the turbulent flame surface area ratio. The term in braces is only dependent on properties of the laminar flamelet and the turbulent time scale of the flow. The expression (4) has been chosen such that for $\ell_{f,t}$ being in equilibrium with the integral length scale of the surrounding flow, turbulent burning velocity expressions as presented in [12] again are recovered. The laminar flame thickness is defined with respect to the ratio of the thermal conductivity and the heat capacity of the flame, evaluated at the position at the inner layer of the flame:

$$\ell_f = \frac{1}{\rho_u s_L}\left.\frac{\lambda}{c_p}\right|_0\ , \quad (5)$$

where ρ_u indicates the unburnt gas mixture density and '0' refers to the inner layer position.

Symbol	Value	definition/origin
a_4	0.37	Bray [3]
b_1	2.0	experimental data [1]
b_3	1.0	experimental data [4]
c_0	0.44	$= C_{\varepsilon 1} - 1$, [11]
c_1	4.63	DNS, [18]
c_2	1.01	$= \sqrt{\frac{3c_\mu c_s}{4\mathrm{Sc}_t}}\frac{c_1 b_3^2}{b_1}$
c_3	4.63	$= c_1 b_3^2$
c_s	2.0	[10, 11]
Sc_t	0.7	

Table 1: Constants for the level set based turbulent premixed combustion model.

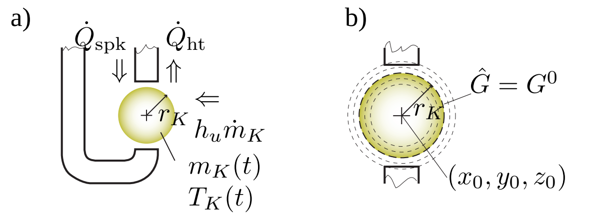

Figure 1: a) Energy balance between the spark plug electrodes and the spark kernel. b) Connection between spark kernel radius r_K and filtered $\widehat{G}$-field.

The turbulent diffusivity in the curvature term of eqn. (1) in this work is expressed in analogy to a mixing length approach as

$$D'_t = \sqrt{\frac{c_\mu c_s}{2\mathrm{Sc}_t}}\ell_{f,t}k^{1/2}\ , \quad (6)$$

therefore the magnitude of the modification of the turbulent burning velocity due to curvature of the mean flame front is dependent on the thickness of the turbulent flame. The constants in eqn. (6) again are chosen such that for a state of equilibrium with the turbulent flow, the standard relationship for the turbulent diffusivity of a scalar, $D_t = \nu_t/\mathrm{Sc}_t$, is obtained.

Spark ignition modeling

For the spark ignition model, the same physical modeling assumptions are used as for turbulent premixed flame propagation in 3D space with respect to the turbulent burning velocity and the expression for the variance (2). Additionally, kernel expansion effects due to electrical spark energy and the effect of kernel curvature will be accounted for. The thermodynamical analysis is carried out similar to Tan [17]. As a first approximation of the model it is assumed that the initial spark kernel is spherical with a given initial position and radius. During the growth of this kernel to a fully turbulent flame the kernel will be assumed to be subjected to convection of the background flow.

The energy balance depicted in figure 1a reads

$$\dot{Q}_{\mathrm{spk}} + \dot{Q}_{\mathrm{chem}} - \dot{Q}_{\mathrm{ht}} = \frac{\mathrm{d}H}{\mathrm{d}t} - h_u \dot{m}_K - V \frac{\mathrm{d}p}{\mathrm{d}t} , \quad (7)$$

where H represents the spark thermal and plasma enthalpy. $\dot{Q}_{\mathrm{spk}}$ denotes the gross electrical energy transfer from the electrodes and $\dot{Q}_{\mathrm{ht}}$ the heat loss to the electrodes. $\dot{Q}_{\mathrm{chem}}$ accounts for the heat release caused by combustion. h_u denotes the specific enthalpy of the unburnt gas mixture which is added to the spark by (laminar or turbulent) flame propagation through the mass stream $\dot{m}_K$.

The effect of spark energy deposited into the kernel and heat losses to the electrodes are related to each other thus forming an effectivity coefficient η_{eff}, in the following assumed to be approximately 0.3:

$$\dot{Q}_{\mathrm{ht}} \approx (1 - \eta_{\mathrm{eff}}) \dot{Q}_{\mathrm{spk}} . \quad (8)$$

The equation of continuity gives the following ordinary differential equation for the increase of spark kernel mass:

$$\frac{\mathrm{d}m_K}{\mathrm{d}t} = \dot{m}_K = 4\pi r_K^2 \, \rho_u s_{T,\kappa} . \quad (9)$$

Here r_K is the radius of the kernel and $s_{T,\kappa}$ an expression for the flame propagation which takes into account the turbulent burning velocity and the effect of laminar and turbulent kernel curvature as done in equation (1). The radius can be readily obtained by

$$r_K = \sqrt[3]{\frac{3m_K}{4\pi\rho_b}} ; \quad (10)$$

however, the density of the gas in the spark ρ_b needs to be known which is – depending on ignition conditions – lower than the density of adiabatically burned gas due to plasma effects of the electrical energy which cause an increased kernel temperature. In order to approximate this temperature T_K eqn. (7) needs to be further modified.

The derivative of the kernel enthalpy gives

$$\frac{\mathrm{d}H}{\mathrm{d}t} = \dot{m}_K h_K + \dot{h}_K m_K \quad (11)$$

and the heat release due to premixed combustion can be expressed as

$$\dot{Q}_{\mathrm{spk}} = \dot{m}_K (h_{\mathrm{ad}} - h_u) . \quad (12)$$

The burning velocity $s_{T,\kappa}$ – modified by curvature effects – can be deduced from (1), in which the curvature of the spherical kernel amounts to $\kappa = 2/r_K$.

$$s_{T,\kappa} = s_T - \frac{2}{r_K} D'_t \quad (13)$$

An equation describing the thickness of the flame brush can be deduced from (2) by assuming uniform turbulent

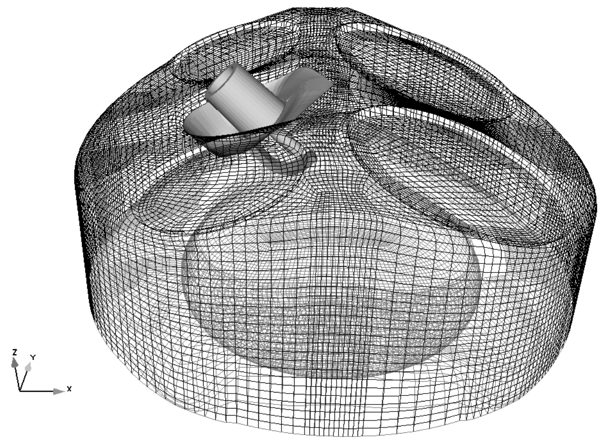

Figure 2: Unstructured computational grid of the closed engine geometry highlighting the modeled spark plug. This mesh comprises 302,000 grid cells.

Bore	$86\,\mathrm{mm}$
Stroke	$86\,\mathrm{mm}$
Displacement	$0.5\,\mathrm{L}$
Compression Ratio	10.3
Engine speed	$2000\,\mathrm{rpm}$
MAP	$95\,\mathrm{kPa}$
Intake mixture:	propane/air w. $\phi = 0.6$
Spark Timing	$40°$BTDC
Spark Energy	$60\,\mathrm{J/s}$
Initial Spark Radius	$r_{K,0} = 1\,\mathrm{mm}$

Table 2: Operating parameters of the engine

profiles:

$$\frac{\mathrm{d}\widetilde{G''^2_{\mathrm{spk}}}}{\mathrm{d}t} = 2\hat{D}_{t,\,\mathrm{spk}} - c_s \frac{\varepsilon}{\hat{k}_{\mathrm{spk}}} \widetilde{G''^2_{\mathrm{spk}}} \quad (14)$$

For engine combustion $\widetilde{G''^2} = \widetilde{G''^2_{\mathrm{spk}}} = 0$ as initial condition. The spark only sees only those turbulent eddies which are smaller equal diameter of the eddy itself. When the flame kernel reaches a specified size $r_{K,\mathrm{end}}$, the model is switched to the 3D equations.

Results

Basis of the model computation is a optical test engine operated in homogeneous charge mode fueled with a lean propane/air mixture [6]. The operating parameters are listed in table 2. The numerical computations were carried out by the code AC-FluX by Advanced Combustion GmbH, a Finite Volume based CFD simulation tool that operates on unstructured meshes and is able to perform adaptive local grid refinement during calculation.

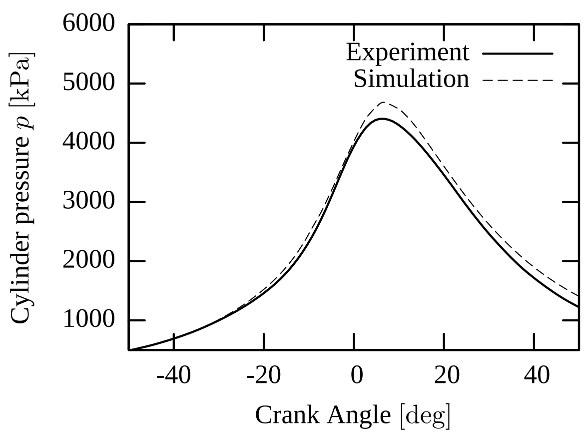

Figure 3: Comparison of cylinder pressures

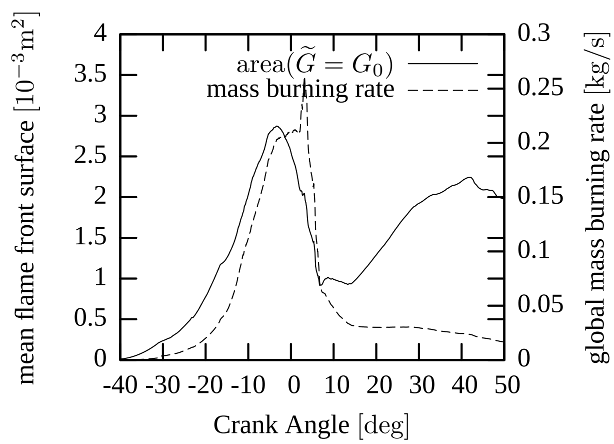

Figure 4: Plot of the mean flame front surface (measured on the left ordinate) and the global mass burning rate (measured on the right ordinate) during the combustion phase.

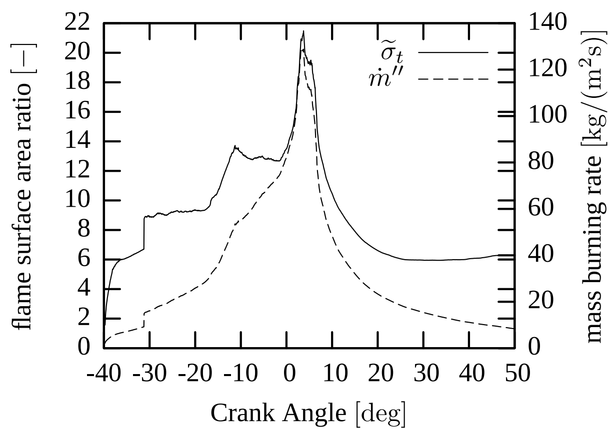

Figure 5: Qualitative comparison of turbulent flame surface area ratio $\widetilde{\sigma}_t$ area weight averaged on the $\widetilde{G} = G_0$ surface (left ordinate) and the area weight averaged flame surface area mass burning rate $\dot{m}''$ (right ordinate).

The simulation was carried out employing two meshes, one with the intake ports modeled. After intake valve closure, the calculation was interrupted at 90°BTDC and the solution at this time step was mapped onto a new grid featuring a closed geometry which is shown in figure 2.

For the laminar flamelet calculation, laminar burning velocity correlations according to Müller *et al.* [7] were employed with a correction of the burnt gas temperature in order to account for the effects of rest gas in the previous cycle, which was assumed here otherwise as inert. For the flame diffusivity λ/c_p, the correlation for hydrocarbons due to [14] was used as basis.

In figure 3, a comparison of measured and calculated cylinder pressure is depicted. In figure 4 both the evolution of the mean flame front surface and the global mass burning rate are plotted. It can be seen, even although both quantities cannot be directly compared to each other quantitatively, the increase in mass burning is preceded by the increase in surface of the mean flame front. This can be explained by the fact that initially, flame propagation is close to laminar and it takes approximately 5°CA after ignition to develop turbulent flame propagation. The area of the mean flame front surface $\widetilde{G} = G_0$ increases until about -3°CA while the heat release increases until approx. 2°CA ATDC. This can be explained by most parts of the flame coming into contact with the wall region. After that, another increase of mean flame front surface can be observed, which does not contribute to a repeated increase in flame surface because the flame propagates in the squish region. Shortly after TDC, a sharp peak in mass burning rate is observed. 3D image analysis of the simulation shows that at TDC (see figure 8b) in the in-cylinder region opposing the spark plug a substantial area of the mean flame front surface is visible that is rapidly reduced by flame propagation when the flame burns out in this region and continues to propagate into the squish region further. This observation is also supported by the slope of the $\mathrm{area}(\widetilde{G} = G_0)$ plot in figure 4, which shows at the same time a steep decrease.

These observations are also supported by the results displayed in fig. 5. The quantity $\dot{m}''$ is equal to the mass burning rate (ρs_T), averaged on the total mean flame surface area. Also the turbulent flame surface area ratio $\widetilde{\sigma}_t$ is averaged over the total mean flame surface area. It can be seen that the profile of $\widetilde{\sigma}_t$ predicts the evolution of the laminar flame kernel into a moderately turbulent flame to take place within 5°CA. As a comparison, the turbulent time scale k/ε at the spark plug immediately prior to ignition spans for this engine speed 13°CA. Immediately after Top Dead Center (TDC), both maximum values of averaged $\widetilde{\sigma}_t$ and mass burning rates are reached which coincide with the location of maximum heat release.

The main mechanism that drives the development of

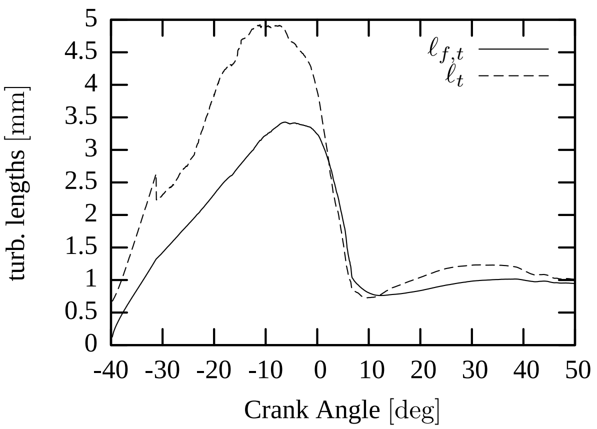

Figure 6: Comparison of turbulent flame brush thickness $\ell_{f,t}$ and turbulent length scale $\ell_{f,t,\mathrm{alg}}$ averaged on the mean flame front surface.

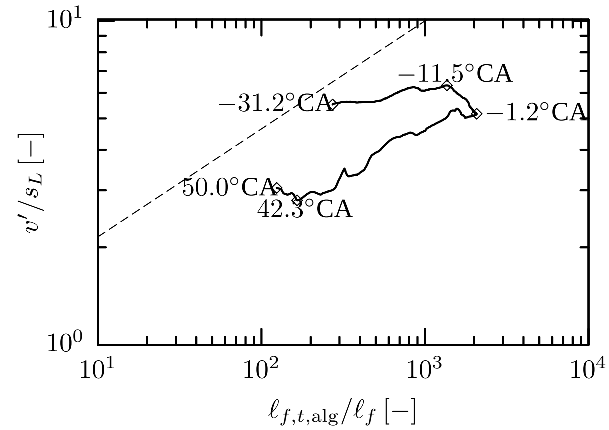

Figure 7: Combustion regime diagram. The dashed line indicates the boundary between the corrugated flamelets which is on the lower right section of the plot and the thin reaction zones regime at the upper left.

the turbulent flame can be explained by the comparison of the turbulent flame brush thickness $\ell_{f,t}$ with the turbulent length scale. In order to facilitate the comparison, a turbulent length scale is defined for this purpose assuming production=dissipation and neglecting the temporal and spatial derivatives in eqn. (2). The result is the "algebraic flame brush thickness"

$$\ell_{f,t,\mathrm{alg}} \equiv \sqrt{\frac{2c_\mu}{c_s \mathrm{Sc}_t}}\,\frac{k^{3/2}}{\varepsilon}\,. \tag{15}$$

Both the turbulent length scale and the flame brush thickness are again averaged over the mean flame front surface area and therefore describe the turbulent scale that the flame sees. Both quantities are increasing in time, while the turbulent flame brush thickness due to the initial condition starts at zero and remains smaller than the turbulent length until immediately after TDC. This is explained by the spatial distribution of the turbulent scales, which are small in vicinity to the wall and also in the region of the spark plug and increase towards the inner region of the combustion chamber. The flame therefore is ignited in regions where small turbulent eddies prevail and then later on expands into regions with larger turbulent eddies. The turbulent flame brush thickness requires time to follow that increase in turbulent length.

The combustion regime in which the engine operates in that mode is depicted in figure 7. The ratios v'/s_L and $\ell_{f,t,\mathrm{alg}}/\ell_f$ are logarithmically averaged over the mean flame front surface. The average of these quantities indicate that the combustion predominantly takes place in the corrugated flamelets regime [11]. Until TDC the dimensionless turbulence intensity v'/s_L remains approximately constant. After this point, this quantity decreases again since the flame burns out close to the wall and propagates in the squish region.

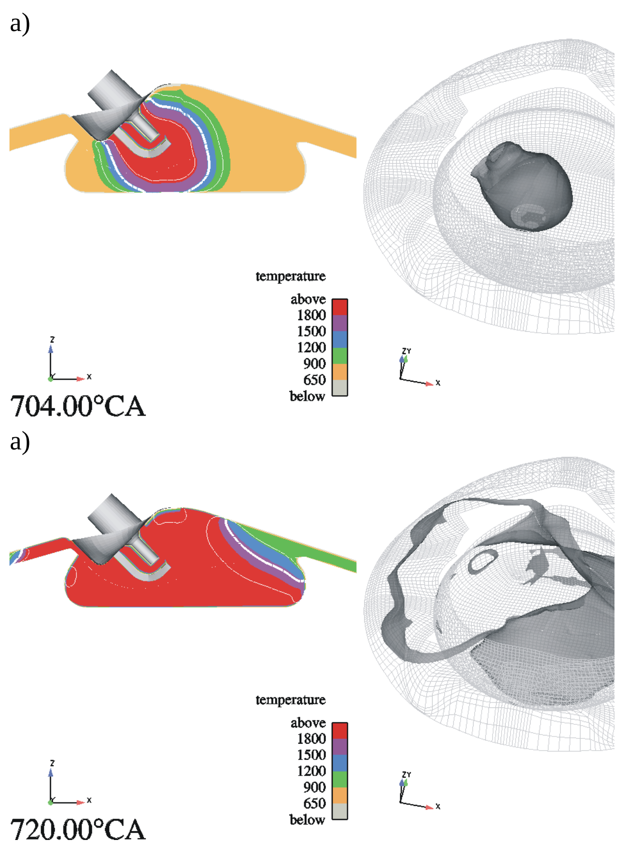

Figure 8: Two plots of the combustion progress in the engine each at two different crank angle degrees. On the left plots a vertical cut through the center of the chamber, showing the spark plug geometry is displayed along with the color coded mean temperature. By solid white lines both the mean flame front $\widetilde{G} = G_0$ (thick line) and the boundary of the flame brush region (thin lines is displayed).

Acknowledgements

The authors gratefully acknowledge the contribution of the engine data by Andreas Lippert, Todd Fansler, and Michael Drake and the computational mesh by Mark Huebler, all from the Powertrain Systems Research Lab, General Motors R&D in Warren, MI.

References

[1] R. G. Abdel-Gayed and D. Bradley. A two-eddy theory of premixed turbulent flame propagation. *Phil. Trans. of the Royal Soc. of London A*, 301(1457):1–25, 1981.

[2] D. Adalsteinsson and J. A. Sethian. The fast construction of extension velocities in level set methods. *Journal of Computational Physics*, 148:2–22, 1999.

[3] K. N. C. Bray. Studies of the turbulent burning velocity. *Proc. Roy. Soc. Lond.*, A 431:315–335, 1990.

[4] G. Damköhler. Der Einfluss der Turbulenz auf die Flammengeschwindigkeit in Gasgemischen. *Zeitschr. f. Elektrochemie*, 46(11):601–626, 1940.

[5] M. Dekena and N. Peters. Combustion modeling with the G-Equation. *Oil & Gas Sci. Tech. – Rev. IFP*, 54(2):265–270, 1999.

[6] A. M. Lippert, T. D. Fansler, and M. C. Drake. High-speed imaging and CFD modeling of sprays and combustion in a spray-guided spark ignition direct injection engine. In *6th Int. Symp. on Internal Combustion Diagnostics*, Baden-Baden, Germany, June 15–16 2004.

[7] U. C. Müller, M. Bollig, and N. Peters. Approximations for burning velocities and markstein numbers for lean hydrocarbon and methanol flames. *Combust. Flame*, 108:349–356, 1997.

[8] S. Osher and R. Fedkiw. *Level Set Methods and Dynamic Implicit Surfaces*. Springer, 2003.

[9] N. Peters. *Fifteen Lectures on Laminar and Turbulent Combustion*. Ercoftac Summer School, September 14-28 1992. Institut für Technische Mechanik, RWTH Aachen, 1992.

[10] N. Peters. A spectral closure for premixed turbulent combustion in the flamelet regime. *J. Fluid Mech.*, 242:611–629, 1992.

[11] N. Peters. The turbulent burning velocity for large scale and small scale turbulence. *J. Fluid Mech.*, 384:107–132, 1999.

[12] N. Peters. *Turbulent Combustion*. Cambridge University Press, 2000.

[13] J. A. Sethian. Fast marching methods. *SIAM Review*, 41(2):199–235, 1999.

[14] M. D. Smooke and V. Giovangigli. Formulation of the premixed and nonpremixed test problems. In M. D. Smooke, editor, *Reduced Kinetic Mechanisms and Asymptotic Approximations for Methane-Air Flames*, volume 384 of *Lecture Notes in Physics*, pages 1–28. Springer-Verlag, 1990.

[15] Z. Tan, S. C. Kong, and R. D. Reitz. Modeling premixed and direct injection SI engine combustion using the G-equation model. *SAE Technical Paper Series*, no. 2003-01-1843, 2003.

[16] Z. Tan and R. Reitz. Modeling ignition and combustion in spark-ignition engines using a level set method. *SAE Technical Paper Series*, no. 2003-01-0722, 2003.

[17] Z. Tan and R. D. Reitz. Development of G-Equation combustion model for direct injection SI engine simulations. In *13th Int. Multidim. Engine Modeling User's Group Meeting*, Detroit, MI, March 2 2003.

[18] H. Wenzel. *Direkte numerische Simulation der Ausbreitung einer Flammenfront in einem homogenen Turbulenzfeld*. Dissertation, RWTH Aachen University, 2000.

[19] F. A. Williams. Turbulent combustion. In J. Buckmaster, editor, *The Mathematics of Combustion*, pages 97–131. SIAM, Philadelphia, 1985.